JOURNAL OF APPLIED ELECTROCHEMISTRY 24 (1994) 439–448

Effect of complexing agent (citric acid) and pH on the cathodic deposition of As–Sb alloys

S. CATTARIN, F. FURLANETTO, M. M. MUSIANI*
IPELP CNR, 4 Corso Stati Uniti, 35020 Camin (PD), Italy

P. GUERRIERO
ICTIMA CNR, 4 Corso Stati Uniti, 35020 Camin (PD), Italy

Received 8 July 1993; revised 31 August 1993

As–Sb alloys have been cathodically deposited onto nickel electrodes from acidic aqueous solutions containing citric acid. The effect of complexing agent concentration, pH, angular speed of the RDE and temperature on deposition rate and alloy composition have been monitored. Increasing citric acid concentration and pH decrease the deposition current and the antimony content of the alloys (measured by EDX analyses). The opposite effect is observed when rotation speed or temperature are increased. Under most combinations of citric acid concentration and pH, the steady-state i/E curves show the current peak already observed in a previous investigation. The morphology and structure of the alloys have been studied with scanning electron microscopy and X-ray diffraction. Alloys containing $\geqslant 74\%$ Sb were found to be crystalline (hexagonal system).

1. Introduction

The cathodic deposition of As–Sb alloys from aqueous citric acid solutions has been studied in our laboratory [1, 2] as one of the necessary steps for preparing thin films of ternary III–V compound semiconductors, like $InAs_xSb_{1-x}$ [3]. The influence of potential and As(III)/Sb(III) ratio in the electrolytic solutions on the alloy composition and deposition kinetics has been studied and described by a kinetic model which satisfactorily accounts for both the steady-state and a.c. impedance results [2]. The presence of a complexing agent was neglected in the model development.

When electrodeposition is performed from solutions containing complexing agents (citric acid in our case) their concentration is known to be of primary importance in determining the alloy composition and its variation with potential; alloy composition is affected by variations in the complexing agent concentration, even when it is present in excess of the metal ions [4]. The alloy composition depends strongly on complexing agents in the case of the so-called mixed-type solutions, i.e. those solutions in which either the two ions are complexed by different chemicals or only one is complexed and the other is a simple ion. Instead, no great effect on alloy composition is expected for the single complex deposition baths where both ions form complexes with the same ligand. The data on the polarographic reduction of As(III) and Sb(III) ions from citric acid media [5], showing a negative shift of the reduction potential of both elements, might suggest that the system under investigation is a single complex case. However, literature on either As(III) or Sb(III) citrate complexes does not allow a conclusive judgment on this point: the electrodeposition of antimony [6–10] and its alloys (see [10] and references therein) from citrate media is extensively described in the literature, whereas arsenic is most effectively deposited from solutions devoid of complexing agents [11, 12]. Furthermore, comprehensive coordination chemistry reviews [13, 14] mention neither arsenic nor antimony citrate complexes, in contrast with many trivalent cations, bismuth included.

Solution pH also has a marked, often unpredictable, effect on alloy composition [4]. Some effect must be expected when the elements to be deposited are in the form of oxygen containing species subject to acid-base equilibria: this is the case of both arsenic and antimony [15]. In addition, solution acidity influences complex formation, especially when the complexing agent itself undergoes acid-base reactions.

For the above reasons, a study of the effect of citric acid concentration on As–Sb alloy deposition appeared interesting, not only for a better elucidation of the essential features of this process, but also in view of its optimization and extension to more complex codeposition cases, like, e.g., the single-step deposition of $InAs_xSb_{1-x}$, at present investigated in our laboratory. The present paper reports on the results of this study, also providing some new data on the effect of operating variables like temperature and electrode rotation rate. In a final section, the

* Corresponding author.

0021-891X

results of a SEM and X-ray diffraction characterization of the morphology and structure of As–Sb alloys is reported.

2. Experimental details

Electrodeposition solutions were prepared from analytical grade $NaAsO_2$, $SbCl_3$, and citric acid, used without further purification. Cyclic voltammetry and chronoamperometry, the latter used to build steady-state i/E curves [1], were performed on nickel rotating disc electrodes (RDE, 0.283 cm^2 area). Potentiostatic depositions of the alloy samples submitted to SEM–EDX analysis were performed, in most cases, on stationary rectangular nickel-plated copper sheet electrodes (3 cm^2 area). The same samples were also used for the X-ray diffraction studies. In the study of the effect of rotation rate on the composition of the deposited alloy, nickel RDE were employed, the 7 mm high head of which could be screwed on the SEM–EDX sample holder.

SEM–EDX analyses were performed on the sample surface (typically on a 10^4 μm^2 area) with an EDAX PV99 energy-dispersive X-ray spectrometer. Because of the deposit thickness (3–5 μm), standardless quantitative analyses were performed with ZAF corrections for bulk samples.

Current efficiency (QE) was computed from deposition charge (Q), deposit mass (W) and composition (X = Sb atomic fraction) according to the formula

$$QE = 100W3F/Q[XW_{Sb} + (1 - X)W_{As}]$$

where W_{Sb} and W_{As} are Sb and As atomic masses.

Solutions were stirred, except when an RDE was used, in contact with atmosphere and thermostated at 25° C, unless differently specified. All potentials are referred to the saturated calomel electrode (SCE). Potential was corrected for ohmic drop in those cases where the results obtained with electrolytes of markedly different resistance were compared (see Figure captions). More details on experimental equipment and procedures may be found elsewhere [1, 2, 16, 17].

3. Results

In previous papers on the cathodic codeposition of As–Sb alloys [1, 2] it was mentioned that satisfactory deposits were obtained under the following set of conditions: total As(III) + Sb(III) ion concentration 0.08 M, citric acid 0.6 M, pH 0.9, room temperature, stirred aerated solutions. In the present work, the As–Sb codeposition has been studied by varying the experimental parameters around the above values.

To understand the effect of the experimental variables on the codeposition process it is generally advisable to investigate their effect on the deposition of each element. Therefore, some data on the effect of pH and citric acid concentration on the deposition of single elements is presented here, since the literature on antimony deposition from citrate baths [6–10] provides little kinetic information and no literature exists, to our knowledge, on the deposition of arsenic from such a medium. In any case, the present paper is mainly devoted to the alloy deposition. Antimony deposition may be investigated by steady-state methods, but a well-defined steady-state cannot be observed in the arsenic deposition [13], so that mainly linear sweep voltammetry data are presented for this element.

3.1. *Deposition of single elements*

3.1.1. Antimony. In our experience, dissolution of $SbCl_3$ to give 0.08 M concentration requires, in the absence of complexing agents, strongly acidic medium (pH < 0). The fact that dissolution occurs rapidly in a 0.6 M citric acid solution, the spontaneous pH of which is 1.6, strongly suggests that complexation of antimony ions occurs. According to the acidity constants found in the literature [18], a 0.6 M citric acid solution contains essentially undissociated citric acid (about 95%) and its monoanion. Open questions remain on the number of protons released by citric acid upon complex formation, and on whether the Sb(III) ion involved in the complex contains oxygen, although citric acid solutions of Sb(III) have been much used for antimony and antimony alloys electrodeposition [6–10].

A titration curve obtained on a solution containing 1 mM citric acid and $SbCl_3$ is shown in Fig. 1 (curve 2) and compared with that of pure 1 mM citric acid (curve 1). The initial pH is lower in the presence than in the absence of $SbCl_3$, a result consistent with both complex formation and $SbCl_3$ hydrolysis. The titration curves show well-defined equivalent points, located in both cases in the same pH range. Curve 2 shows that the mixture requires 6 mmol of NaOH to reach the only equivalent point observed. This result

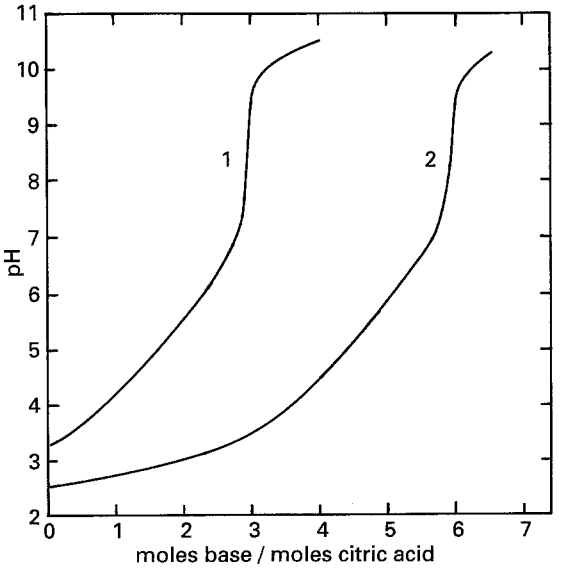

Fig. 1. Titration curves of 10^{-3} M citric acid (1) and 10^{-3} M citric acid + 10^{-3} M $SbCl_3$ (2) with 10^{-2} M NaOH.

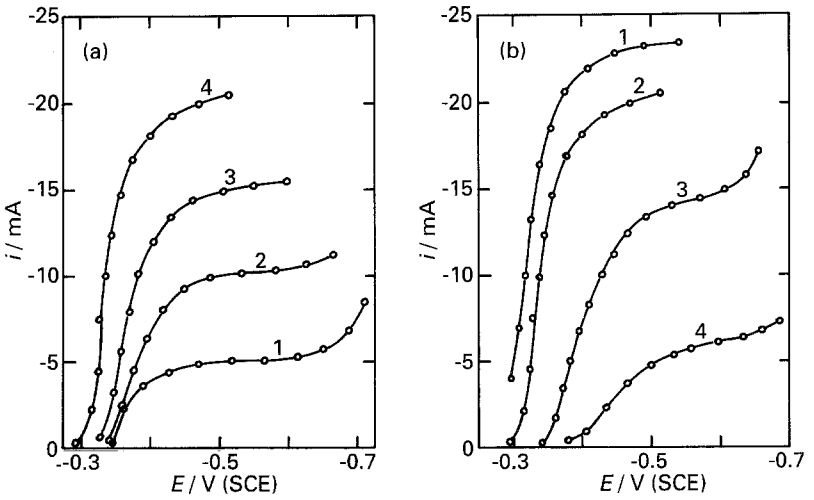

Fig. 2. Steady-state i/E curves for the deposition of antimony onto nickel RDE (1000 r.p.m.) from citric acid solutions with various [citric acid]/[$SbCl_3$] ratios. (a) Citric acid 0.6 M, pH 0.9, $SbCl_3$ 0.02 (1), 0.04 (2), 0.06 (3) and 0.08 M (4). (b) $SbCl_3$ 0.08 M, pH 0.9, citric acid 0.3 (1), 0.6 (2), 1.2 (3) and 2.4 M (4). Potentials were corrected for ohmic drop.

suggests that at the pH value corresponding to the equivalent point, the antimony citric acid complex is no longer present, so that the overall reaction may be written:

$$SbCl_3 + H_3L + 6NaOH = Na_3L + Sb(OH)_3 + 3NaCl + 3H_2O$$

where H_3L and Na_3L are citric acid and its trisodium salt. Such a behaviour is at variance with that observed for Al(III)-citric acid complex [19], in which case citric acid is displaced by hydroxyls only at much higher pH.

The effect of citric acid/Sb(III) concentration ratio on the deposition of antimony was studied by either varying $SbCl_3$ or citric acid amount, while keeping constant the concentration of the other chemical. Figure 2 shows the results of both sets of experiments (curves in Fig. 2 are corrected for the ohmic drop, since the ohmic resistance markedly changed with citric acid concentration, being higher for the more concentrated solutions having much larger viscosity). At constant citric acid concentration, a plateau current proportional to the $SbCl_3$ concentration is observed, Fig. 2(a), for very negative E values, where antimony deposition is under diffusion control [1]. Below the plateau (less negative E) the i/E curve shifts towards negative E as the citric acid/$SbCl_3$ ratio increases. At constant $SbCl_3$ concentration, besides the potential shift observed below the diffusion plateau, a decrease in the limiting current with increasing citric acid concentration is observed, Fig. 2(b). This result is largely due to the viscosity increase of the solution: the limiting current of the $[Fe(CN_6]^{3-}$ reduction was found to decrease by a factor of 2.7 upon changing the concentration of added citric acid from 0.3 to 2.4 M. The residual effect might be due to the formation of complex ions involving more than one ligand at higher absolute concentrations.

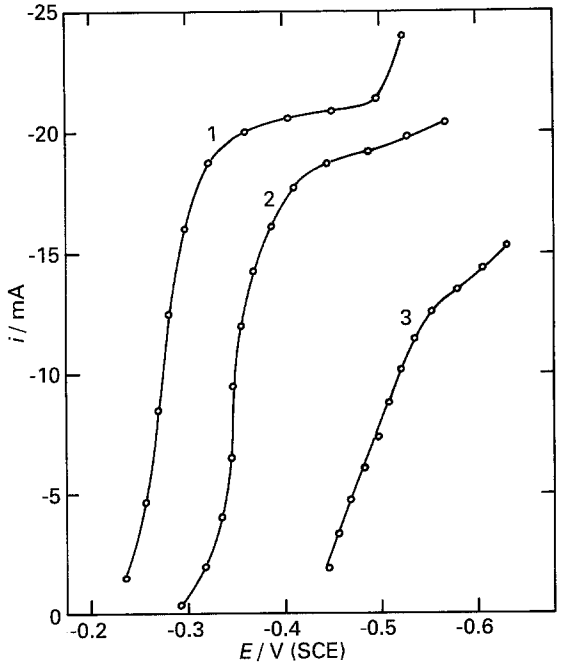

Fig. 3. Steady-state i/E curves for the deposition of antimony onto nickel RDE (1000 r.p.m.) from 0.6 M citric acid + 0.08 M $SbCl_3$ solutions at various pH values: 0.6 (1), 0.9 (2) and 1.6 (3). Potentials were corrected for ohmic drop.

Figure 3 shows steady-state curves for the deposition of antimony from citric acid solutions obtained at pH values in the range 0.6–1.6 (ohmic drop corrected). A pH increase shifts the deposition potential towards negative E. The equilibrium potential of the reaction

$$SbO^+ + 2H^+ + 3e^- = Sb + H_2O$$

undergoes a 40 mV per (pH unit) shift in the negative direction, which increases to 60 mV per (pH unit) if $HSbO_2$ is considered [15]. The experi-

Table 1. Current efficiency for antimony deposition at various pH and E values

E/V vs SCE	*Current efficiency/%*		
	pH 0.6	*pH 0.9*	*pH 1.6*
−0.3	90	79	
−0.4	94	89	
−0.5	95	92	92
−0.6	94	92	87
−0.7	82	94	89
−0.8	71	94	90
−0.9			89
−1.0			92

Deposition conditions: Citric acid 0.6 M, $SbCl_3$ 0.08 M.

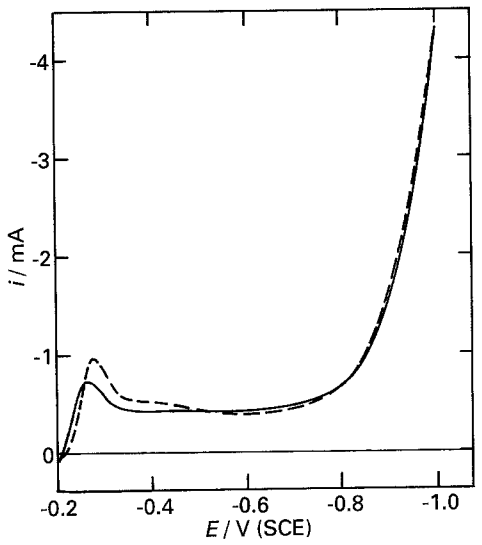

Fig. 4. Linear sweep voltammetries obtained at nickel RDE (1000 r.p.m.) in 0.04 M $NaAsO_2$, pH 0.6 in the absence (solid line) or presence (dashed line) of 0.6 M citric acid. Sweep rate 100 mV s^{-1}.

mentally observed shift is much larger, indicating that pH variation must affect complex formation equilibria.

The current yield of antimony potentiostatic depositions was $\geqslant 90\%$ at all pH values investigated, for appropriate potentials (Table 1).

3.1.2. Arsenic. Linear sweep voltammetries for the deposition of arsenic onto nickel from solutions containing or not citric acid were recorded in the pH range 0.6–1.6; those obtained at pH 0.6 are compared in Fig. 4. Neither the voltammetric peak occurring around −0.3 V, nor the wave present at $E < -0.8$ V show a significant dependence on the presence of citric acid. Relatively thick As deposits can be obtained only at $E < -0.9$ V; the same current efficiency (approximately 50% at $E = -1.0$ V) is measured in the presence and in the absence of citric acid.

The voltammetric curves obtained both in the presence and in the absence of citric acid are affected in the same way by pH variation in the range 0.6–1.6: the peak and the wave undergo comparable shifts towards negative potential at higher pH.

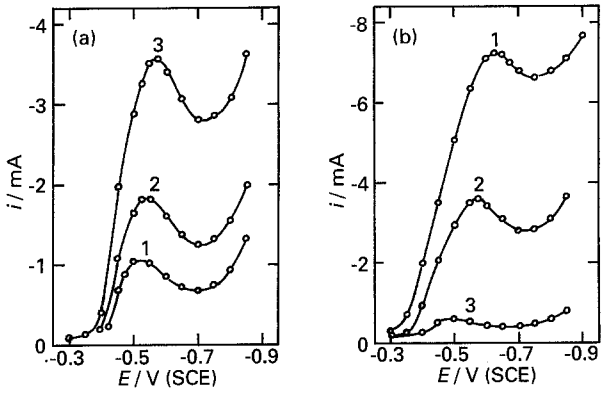

Fig. 5. Steady-state i/E curves for the deposition of As–Sb alloys onto Ni RDE (1000 r.p.m.) from citric acid solutions with $[NaAsO_2] = [SbCl_3]$ and various [citric acid]/$[SbCl_3]$ ratios. (a) Citric acid 0.6 M, pH 0.9, $NaAsO_2$ and $SbCl_3$ 0.02 (1), 0.03 (2), and 0.04 M (3). (b) $NaAsO_2$ and $SbCl_3$ 0.04 M each, pH 0.9, citric acid 0.45 (1), 0.6 (2) and 0.8 M (3).

The electrodeposition experiments performed on single elements clearly indicate a much stronger effect of citric acid on antimony than on arsenic deposition.

3.2. *As–Sb deposition*

3.2.1. Effect of citric acid. Figure 5 shows steady-state current potential curves for the deposition of As–Sb alloys recorded with equimolar amounts of As(III) and Sb(III) ions and various ratios between the concentrations of complexing agent and electroactive ions. The data in (a) and (b) were obtained at fixed citric acid concentration and fixed ion concentration, respectively. The current peak characterizing As–Sb codeposition [1, 2] is observed in all cases. Increasing citric acid relative concentration shifts the curves towards negative potential and decreases the peak current; surprisingly this effect is more marked in Fig. 5(b) (fixed ionic concentration) than in Fig. 5(a). However, also in the latter case, the peak current increases faster than the ion concentration. As already mentioned for the deposition of pure antimony the increased solution viscosity caused by large

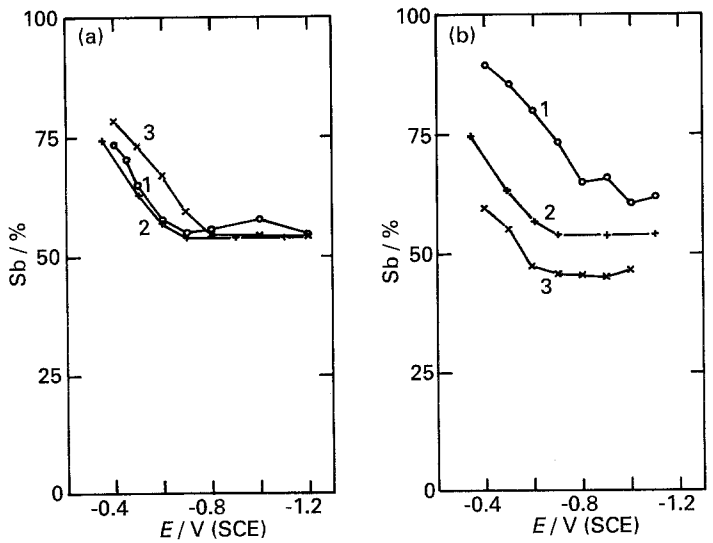

Fig. 6. Composition (Sb at %) of As–Sb alloys obtained from citric acid solutions with $[NaAsO_2] = [SbCl_3]$ and various [citric acid]/$[SbCl_3]$ ratios. (a) Citric acid 0.6 M, pH 0.9, $NaAsO_2$ and $SbCl_3$ 0.02 (1), 0.04 (2), and 0.06 M (3). (b) $NaAsO_2$ and $SbCl_3$ 0.04 M each, pH 0.9, citric acid 0.4 (1), 0.6 (2) and 0.8 M (3).

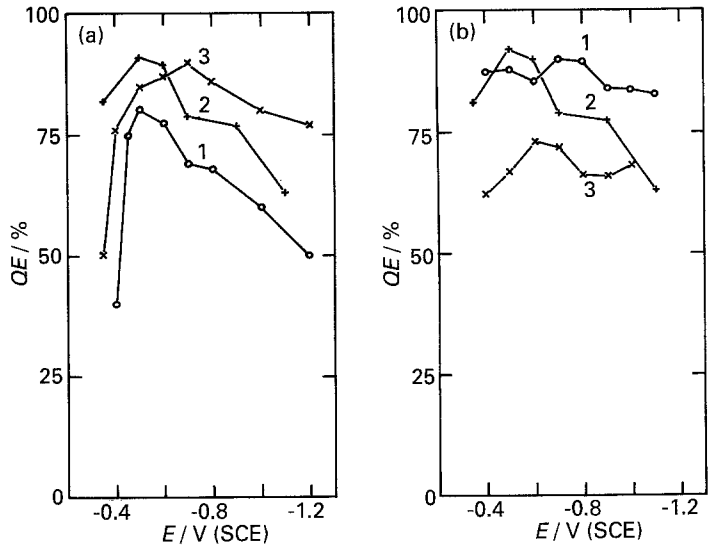

Fig. 7. Current efficiency of the As–Sb alloy deposition from citric acid solutions with $[NaAsO_2] = [SbCl_3]$ and various [citric acid]/$[SbCl_3]$ ratios. (a) Citric acid 0.6 M, pH 0.9, $NaAsO_2$ and $SbCl_3$ 0.02 (1), 0.04 (2), and 0.06 M (3). (b) $NaAsO_2$ and $SbCl_3$ 0.04 M each, pH 0.9, citric acid 0.4 (1), 0.6 (2) and 0.8 M (3).

citric acid concentration may contribute to depress the current.

Figure 6 shows composition potential curves obtained as a function of the citric acid/electroactive ions ratio, by either keeping constant the citric acid (a) or the ions (b) concentration. In all cases the shape of the curves is the same [1]: at low overpotential (less negative E) the deposits are antimony-rich with the antimony amount decreasing for increasing overpotential, while a limiting composition is attained at large overpotential. The general trend is that a high citric acid/electroactive ions ratio opposes the preferential antimony deposition (although an inversion appears in Fig. 6(a) between curves 1 and 2 the values of which, however, differ less than the expected experimental error). Thus, both i/E and composition-E curves show that an increase in the relative amount of citric acid with respect to As(III) and Sb(III) ions (present at equal concentration) produces the same effect as an increase in the As(III)/Sb(III) concentration ratio [2].

A major difference between Fig. 6(a) and (b) is observed in the limiting composition region: at fixed citric acid concentration the curves converge to about the same value, whereas at fixed ion concentration each curve tends to a different composition (well beyond experimental uncertainty).

Figure 7(a) and (b) shows the potential dependence of the current efficiency which tends to be better at higher ion concentration and lower citric acid concentration.

A comparison between As–Sb alloy deposition in the presence and in the absence of citric acid is only possible for solution acidity high enough to prevent antimony ion hydrolysis and antimony oxide precipitation. Thus, the As–Sb deposition from 0.04 M $SbCl_3$, 0.04 M $NaAsO_2$ in 2.5 M HCl was carried out without and with 0.6 M citric acid added. Both the i/E curves (which showed no peak) and the composition-E curves were essentially coincident, suggesting that citric acid exerts no complexing action at this very low pH.

3.2.2. Effect of pH. Figure 8 shows rotating-disc linear-sweep voltammetric curves obtained at various pH values in the same citric acid solution. With the adopted potential sweep and electrode rotation rates, the current measured in the forward and backward sweeps almost overlaps and is not far from the steady state value. The effect of pH is dramatic: deposition current markedly decreases when pH increases. As previously mentioned the peak disappears at the highest acid concentration.

Figure 9 shows the composition-E dependence measured at four different pH values; for the highest pH (1.6) electrodeposition at low overpotentials was very slow; thus, all analysed samples were obtained at $E \leqslant -0.9$ V. At $E \leqslant -1.3$ V, samples were heterogeneous showing dendritic growth of an antimony-richer alloy on and near the sheet edges. The composition of the alloy deposited far from the edges is reported in Fig. 9. At all potentials, including those corresponding to the limiting composition range, low pH values correspond to antimony-richer alloys.

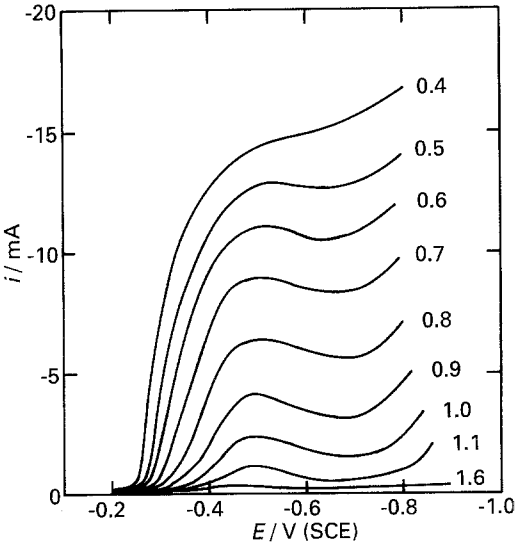

Fig. 8. Linear sweep voltammetries for the deposition of As–Sb alloys onto nickel RDE (1000 r.p.m.) from 0.6 M citric acid + 0.04 M $NaAsO_2$ and 0.04 M $SbCl_3$ solutions at various pH values indicated on the Figure. Sweep rate 10 mV s^{-1}. Potentials were corrected for ohmic drop.

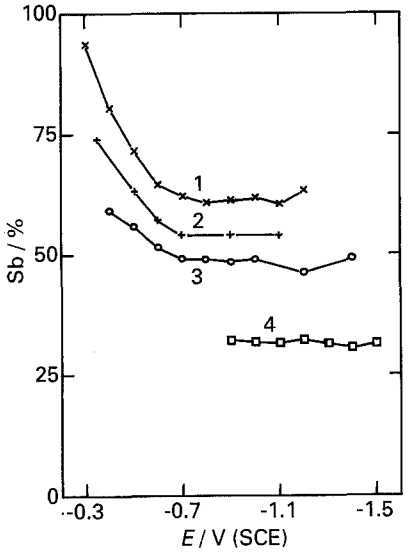

Fig. 9. Composition (Sb at %) of As–Sb alloys obtained from 0.6 M citric acid + 0.04 M $NaAsO_2$ and 0.04 M $SbCl_3$ solutions at various pH values: 0.5 (1), 0.9 (2), 1.1 (3) and 1.6 (4).

Figure 10 shows that the current efficiency is better, and indeed very high, at low pH, except at the most negative potential where hydrogen evolution is a more serious drawback for more acidic solutions. As also seen in Fig. 7, current efficiency is also low at the lowest overpotentials explored. Owing to the heterogeneity of some samples, *QE* for pH 1.6 are reported only for the homogeneous ones.

3.2.3. Effect of mass transfer and temperature. The effect of mass transfer on the alloy composition has been studied on nickel rotating disc electrodes which may be transferred to a SEM and is shown in Fig. 11 (the dependence of the i/E curves on Ω has been described and discussed in a previous paper [2]). Figure 11 shows that alloys deposited under forced convection are richer in antimony than the corresponding alloys obtained on a stationary electrode. This is not only true in the potential

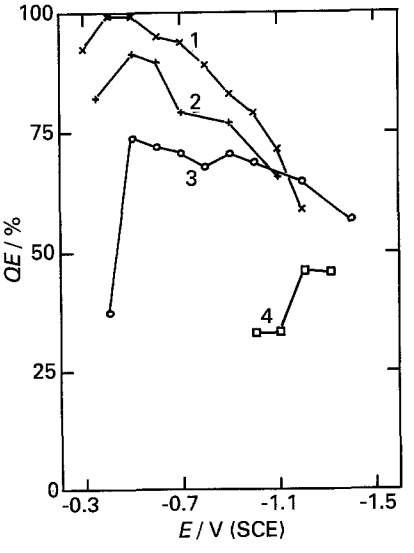

Fig. 10. Current efficiency of the As–Sb alloy deposition from 0.6 M citric acid + 0.04 M $NaAsO_2$ and 0.04 M $SbCl_3$ solutions at various pH values: 0.5 (1), 0.9 (2), 1.1 (3) and 1.6 (4).

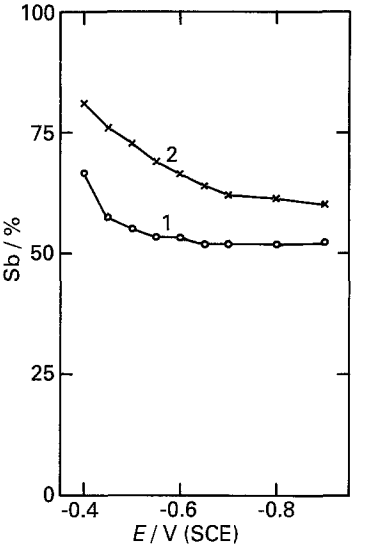

Fig. 11. Effect of mass transfer on the composition (Sb at %) of As–Sb alloys deposited onto nickel RDE from 0.6 M citric acid + 0.04 M $NaAsO_2$ and 0.04 M $SbCl_3$ solutions. RDE angular velocity 0 (1) and 2500 r.p.m. (2).

range where the composition depends on E but also at large negative E, where it is almost potential independent.

The effect of deposition temperature has also been tested, by recording steady-state current potential curves at temperatures above 25° C. It has been found that higher temperatures induce higher currents, without changing the shape of the i/E curves. It has already been shown in [1] that antimony richer coatings are obtained from higher temperature media.

3.3. *Morphology of the deposits and X-ray diffraction study*

Figure 12(a)–(d) shows typical morphologies of As–Sb electrodeposits obtained for increasingly negative potential. At the lowest overpotential the deposits are crystalline (sample (a)), consisting of densely packed crystals a few micrometre in size. On increasing the overpotential, crystals are no longer evident (b), then the deposits become nodular (c) and finally dendritic (d). At all potentials the samples are homogeneously coated. It is significant that deposits of crystalline aspect are only observed under conditions producing antimony-rich alloys (Sb > 80%); thus, at high citric acid concentration and high pH, the deposits look amorphous even at the least negative deposition potential. To the naked eye samples of type (a) appeared dull, those of type (b) bright and those of type (c) and (d) had a powdery aspect and exhibited limited adhesion.

Sb and As–Sb alloys with antimony content in the range 96–67%, all approximately 3 μm thick, were submitted to X-ray diffraction analysis. The data relative to alloy deposits are summarized in Table 2.

Interestingly, sample 3 (74% Sb) was crystalline although its aspect was similar to that of the sample

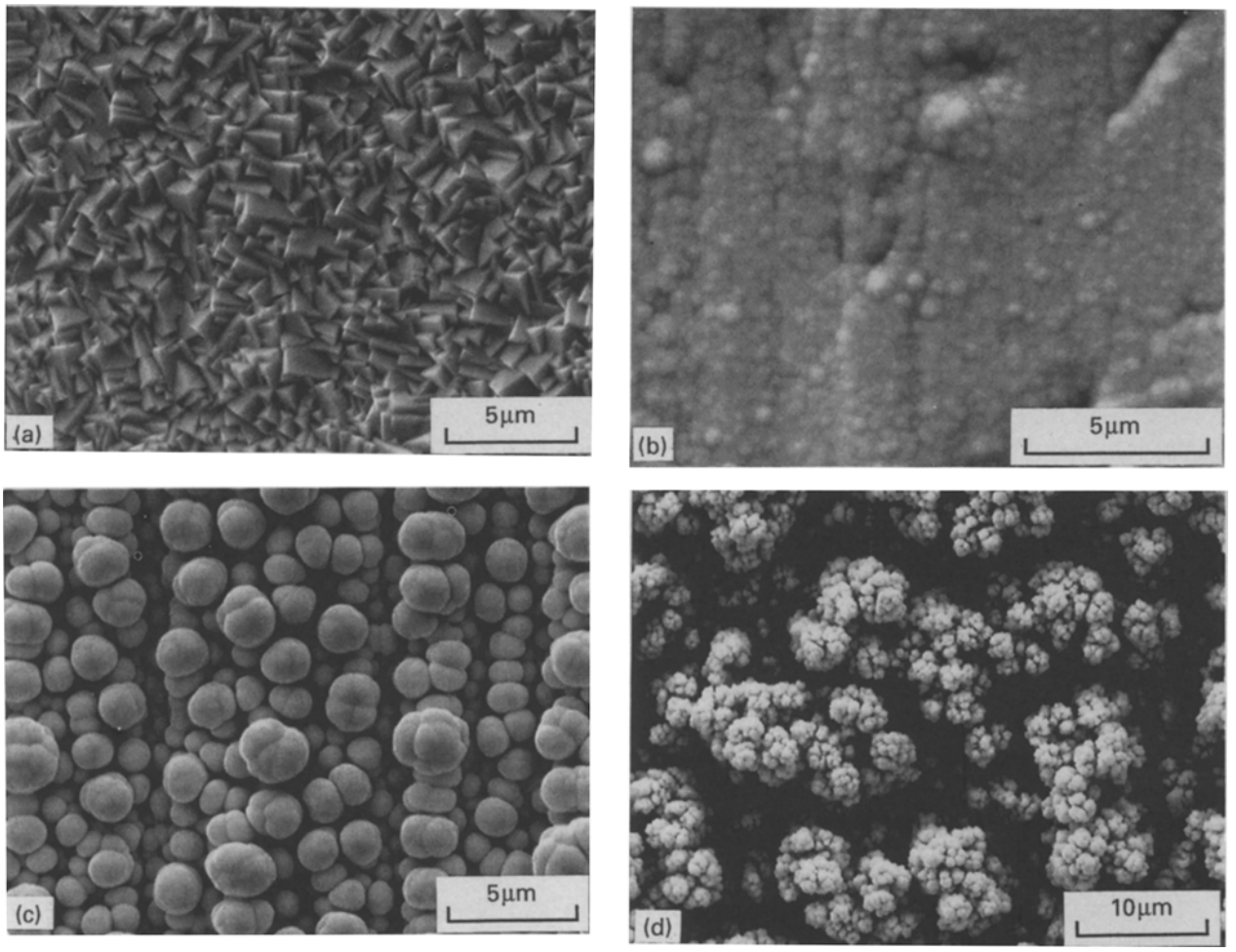

Fig. 12. SEM photographs illustrating typical morphologies of As–Sb alloy deposits obtained with 4–5 C cm^{-2} deposition charge. Depositions were performed from 0.6 M citric acid + 0.04 M $NaAsO_2$ and 0.04 M $SbCl_3$ at pH 0.5 and $E - 0.3$ (a), −0.5 (b) −0.8 (c) and −1.0 V (d).

of Fig. 12(b). All samples with less than 74% antimony were found to be amorphous. However, samples with antimony as high as 82% but prepared at high current density were also amorphous, indicating that crystallinity depends on deposition conditions, not only on composition.

Figure 13 shows the XRD spectrum of sample 2 (91% Sb) compared with the expected peak positions and intensities for antimony. The peaks marked with an asterisk belong to the underlying nickel. All the main expected reflections are visible, although the relative intensities are altered by both preferential orientation and the dependence of the effective sampling depth on Θ. The absence of other peaks shows that a single crystalline phase is formed. The alloys crystallize in the hexagonal system, as both arsenic and antimony do. All experimental reflections are shifted to higher 2Θ values than the corresponding reflections of pure antimony. This shift is due to a contraction of the cell dimension upon replacement of antimony by arsenic. Cell parameters are reported in the fourth column of Table 2. Using Vegard's law which assumes a linear variation of the

Table 2. SEM–EDX and XRD data of electrodeposited As–Sb alloys: morphology, Sb atomic fraction, cell parameters and composition calculated from cell parameters according to Vegard's law

Sample	*SEM aspect*	*Sb % (EDX)*	*Cell parameters /nm*		*Sb% (XRD) from a*	*from c*
			a	*c*		
1	crystalline	96	0.4269	1.119	94.8	87.7
2	crystalline	91	0.4246	1.118	90.5	86.3
3	crystalline	82	0.4210	1.115	84.0	82.2
4	nodular	74	0.4184	1.108	78.9	72.6
5	nodular	67	amorphous		–	–

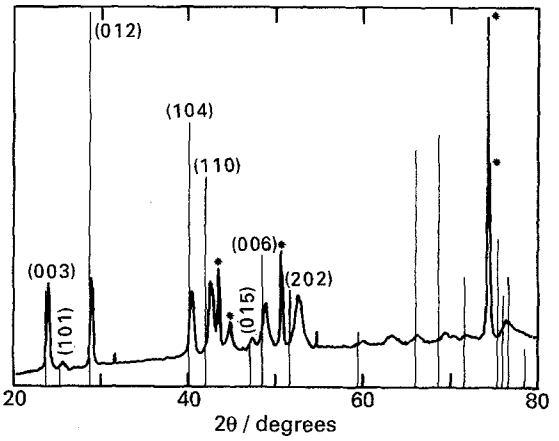

Fig. 13. XRD spectrum of an electrodeposited As–Sb alloy (91% Sb) compared with a literature antimony spectrum [21]. CuK_α radiation.

cell parameters with composition, the antimony content of the alloy may be computed:

$$Sb\% = 100(p_{exp} - p_{As})/(p_{Sb} - p_{As})$$

where p is either a or c parameter. Alloy compositions calculated from XRD data and JCPDS tables [20, 21] are reported in Table 2 (fifth column) and appear in rather good agreement with EDX data, suggesting that the deposited alloys are solid solutions.

4. Discussion

Summarizing the effect of pH, complexing agent concentration, Ω (see [2] for i/E curves) and temperature (see [1] for composition-E curves) on the As–Sb codeposition, one observes that current increase and alloy enrichment in antimony always go together, being caused by low pH, low citric acid, high Ω and high temperature. By studying the effect of these variables on the deposition of single elements we have concluded that antimony is strongly sensitive to citric acid while arsenic is not. A similar dependence of In–Sb alloys composition on the same variables has been observed by Sadana and Singh [22] who found that citric acid affects Sb(III) reduction much more than In(III) reduction. Henceforth data are discussed assuming that the complexing agent only acts on Sb(III).

The observed behaviour may be explained in its main features by simply considering that the antimony deposition potential is made less noble in the presence of citric acid. Since citric acid presumably acts as complexing agent in the form of an anion, its effect on deposition potential is stronger at higher pH. Figure 14 shows i/E curves calculated according to the kinetic model proposed in [2] with kinetic constants corresponding, from curve 1 to 5, to progressively less noble antimony deposition potential. (The current expression is given in the Appendix, while the kinetic model is fully discussed in [2]). The model accounts for several experimental results: when antimony deposition potential becomes less noble owing to complexation, the onset of reduction current shifts to more negative E values, the current peak decreases in size and is slightly shifted towards less negative E. The peak approaches a plateau when the difference in nobility becomes so large that antimony deposition rate attains its limiting value while arsenic deposition rate is still very low.

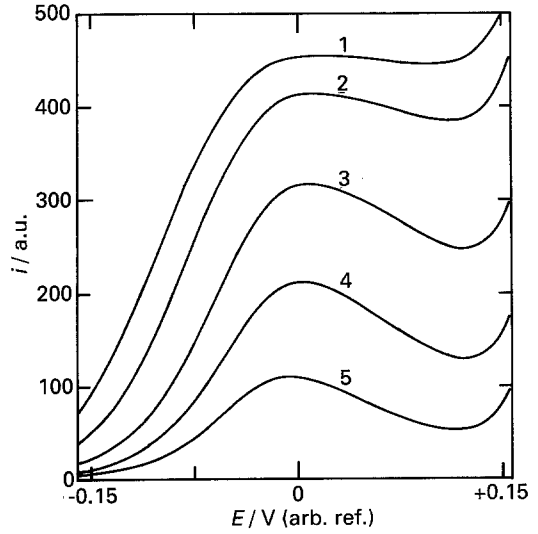

Fig. 14. Steady-state i/E curves for the deposition of As–Sb alloys calculated according to Equation 10 in [2] (see also Equation 1 of the Appendix) with the following set of parameters: b_1 30 V^{-1}, b_2 75 V^{-1}, $k_1'^{\circ}$ (a) 20000, (b) 10000, (c) 5000, (d) 2000 and (e) 1000 cm s^{-1}, $k_1''^{\circ} = k_1'^{\circ}/2000$, $k_2'^{\circ}$ 1 cm s^{-1}, $k_2''^{\circ}$ 0.0005 cm s^{-1}, δ 0.003 cm, and r 1.

The shift of the deposition potential of antimony also explains why the alloys deposited before the limiting region are less antimony rich at high citric acid concentration (Fig. 6) and high pH (Fig. 9). In the same potential region, the effects of both electrode rotation rate (Fig. 11) and temperature also follow a general trend: all factors opposing the depletion of the nobler element at the cathode/solution interface favour its deposition [4].

The effect of the different variables on the composition of the alloys in the limiting potential region, where the constancy of composition (Figs 6 and 9) might suggest that codeposition occurs under diffusion control for both elements, deserves some deeper discussion. According to Brenner [4], who assumes that the same diffusion layer thickness holds for both ions, the atomic ratio between two elements M and N codepositing under limiting current conditions is given by $R = (C_m^* D_m / C_n^* D_n)$, where C^* represent bulk concentration and D diffusion coefficient. If the limiting current at an RDE is considered,

$$i_L = 0.620 nFAD^{2/3}\omega^{1/2}\nu^{-1/6}C^*$$

different diffusion layer thicknesses must be assumed for two ions having different diffusion coefficients. In this case, $R = (C_m^*/C_n^*)(D_m/D_n)^{2/3}$. In both cases, R may only change with an experimental variable if either C^* or D (or both) of at least one ion is sensitive to that variable.

If the following complexation and acid-base equilibria are considered (other possible reactions in which, e.g., Sb(III) ions do not release O might be alternatively considered)

$$SbO^+ + H_3L = SbHL^+ + H_2O$$

$$SbHL^+ = SbL + H^+$$

it is clear that the effective concentration of the species easier to reduce decreases upon increasing citric acid concentration and pH. Complex formation must also be assumed to decrease D. The data in Fig. 2(a) shows, when the complexing ion concentration is constant, that the limiting current for antimony deposition is proportional to Sb(III) concentration, thus suggesting that no change in the nature of the diffusing species occurs under these conditions. In agreement, composition curves in Fig. 6(a) converge at large negative E values. Instead, the curves in Fig. 6(b) do not converge to the same limiting

composition. Besides the possible effects of viscosity discussed hereafter in connection with the dependence of composition on mass transfer rate, it is interesting to stress some correspondence between Figs 2(b) and 6(b). The increase in citric acid concentration depressing the limiting deposition current of pure antimony also depresses the antimony content of the alloys in the limiting composition range.

Figure 11 shows that the electrode processes are sensitive to the hydrodynamic regime which modifies the concentration of reactants and products at the interface. In particular, the reduction of both arsenic and antimony ions (and, for some potential values, parasitic hydrogen evolution) are likely to cause local pH increase at the cathode (any citrate anion freed by the reduction consumes protons by acid-base equilibria). A forced convection may oppose the pH increase in the cathodic region and, therefore, favour antimony deposition. Similarly, higher Ω values should enhance the rate of removal of citric acid produced at the cathode and, again, favour antimony deposition. It is interesting to note that experiments carried out with variable citric acid concentration, and therefore variable viscosity, showed that higher viscosity, inducing slower mass transfer rate, depressed antimony content in the alloys, as the absence of forced convection did.

The effect of temperature is explained by its influence on either mass transfer rate (higher at higher T) or stability of antimony-citric acid complexes (lower at higher T), both inducing higher deposition rate and antimony content at higher T.

In conclusion, the reported experiments show that citric acid medium may be considered a mixed-type solution for deposition of As–Sb alloys, although previous polarographic experiments [5] may suggest the opposite conclusion. The medium appears particularly suitable since deposit composition may be varied over a wide range acting on citric acid concentration, pH and temperature (besides, of course, As(III)/Sb(III) ratio and potential). The deposited alloys are of the solid solution type and are either crystalline or amorphous, mainly depending on their composition.

Appendix

The As–Sb alloy deposition current is given by Equation 10 in [2]

$$i = \frac{3DFCQ_1}{(3DF + \delta Q_1)} + \frac{3DFrCQ_2}{(3DF + \delta Q_2)} \qquad (1)$$

with $Q_1 = (k_1' - k_1'')\Theta + k_1''$ and $Q_2 = (k_2' - k_2'')\Theta + k_2''$. In Equation 1 D is the diffusion coefficient (assumed to be the same for both ions), δ the hydrodynamically controlled diffusion layer thickness, F the Faraday constant, C the Sb(III) ion concentration, and r the ratio between the concentrations of the As(III) and Sb(III) ions in the electrolytic solution. k_1', k_1'', k_2' and k_2'' are the potential-dependent kinetic constants involved in the four elementary electrochemical processes involved in the alloy deposition:

$$k_1' = 3Fk_1'^{\circ}e^{-(b_1E)} \text{ for the reaction}$$

$$Sb^* + Sb(III) + 3e^- = Sb_{bulk} + Sb^*$$

$$k_2' = 3Fk_2'^{\circ}e^{-(b_2E)} \text{ for the reaction}$$

$$Sb^* + As(III) + 3e^- = Sb_{bulk} + As^*$$

$$k_1'' = 3Fk_1''^{\circ}e^{-(b_1E)} \text{ for the reaction}$$

$$As^* + Sb(III) + 3e^- = As_{bulk} + Sb^*$$

$$k_2'' = 3Fk_2''^{\circ}e^{-(b_2E)} \text{ for the reaction}$$

$$As^* + As(III)_+ 3e^- = As_{bulk} + As^*$$

As* and Sb* represent surface sites. Θ is the potential dependent atomic fraction of antimony in the outermost alloy monolayer, varying between 1 and 0 as the potential becomes progressively more negative (see [2] Equation 11):

$$\Theta = \frac{-b \pm \sqrt{b^2 - 4ac}}{2a} \qquad (2)$$

with

$$a = \delta[rk_1'k_2' + (1 - r)k_1''k_2' - k_1''k_2''] \qquad (3)$$

$$b = 3FD(k_1'' + rk_2') + \delta[(r - 1)k_1''k_2' + 2k_1''k_2''] \qquad (4)$$

and

$$c = -k_1''(3FD + \delta k_2'') \qquad (5)$$

Acknowledgments

The authors wish to thank Dr M Gazzano of CSFM CNR Bologna for recording XRD spectra.

References

[1] M. M. Musiani, F. Paolucci and P. Guerriero, *J. Electroanal. Chem.* **332** (1992) 113.
[2] M. M. Musiani and C. Pagura, *J. Electroanal. Chem.* **352** (1993) 197.
[3] G. Mengoli, M. M. Musiani and F. Paolucci, *J. Electroanal. Chem.* **332** (1992) 199.
[4] A. Brenner, 'Electrodeposition of Alloys', Academic Press, New York (1963).
[5] E. J. Breda, L. Meites, T. B. Reddy and P. W. West, *Anal. Chim. Acta* **14** (1956) 390.
[6] K. G. Soderberg and H. L. Pinkerton, *Plating* **37** (1950) 254.
[7] G. R. Schaer, W. H. Safranek and C. L. Faust, *ibid.* **45** (1958) 139.
[8] N. P. Fedot'ev, S. Ya. Grilikhes and I. B. Hapyshkina, *Z. Prikl. Khim.* **32** (1959) 2798.
[9] V. N. Medyanik and G. V. Shula, *ibid.* **49** (1976) 1081.
[10] Y. N. Sadana, J. P. Singh and R. Kumar, *Surf. Technol.* **24** (1985) 319.
[11] A. P. Tomilov and N. E. Chomutov, *in* 'Encyclopedia of the Electrochemistry of the Elements, (edited by A. J. Bard), Vol. II, Marcel Dekker, New York (1975) p. 21.
[12] I. A. Menzies and L. W. Owen, *Electrochim. Acta* **11** (1966) 251.
[13] V. Pyatnitskii, *Russ. Chem. Rev.* **32** (1963) 44.
[14] J. D. Pedrosa De Jesus, *in* 'Comprehensive Coordination Chemistry', (edited by G. Wilkinson, R. D. Gillard, J. A. McCleverty), Vol. 2, Pergamon Press, Oxford (1987) p. 461.

[15] M. Pourbaix, 'Atlas d'Equilibres Electrochimiques', Gautier-Villars, Paris (1963).
[16] F. Paolucci, G. Mengoli and M. M. Musiani, *J. Appl. Electrochem.* **20** (1990) 868.
[17] G. Mengoli, M. M. Musiani, F. Paolucci and M. Gazzano, *ibid.* **21** (1991) 863.
[18] L. G. Sillen and A. E. Martell (eds.), 'Stability Constants of Metal-Ion Complexes', The Chemical Society, London (1964).
[19] R. J. Motekaitis and A. E. Martell, *Inorg. Chem.* **23** (1984) 18.
[20] Joint Committee for Powder Diffraction Standards, Powder Diffraction File International Center for Diffraction Data, Swarthmore, PA (1985), card 35–732.
[21] Joint Committee for Powder Diffraction Standards, Powder Diffraction File International Center for Diffraction Data, Swarthmore, PA (1955), card 5–0632.
[22] Y. N. Sadana and J. P. Singh, *Plat. Surf. Finish.* **64** (1985) 64.